JOURNAL OF PROPULSION AND POWER
Vol. 10, No. 3, May–June 1994

Motor and Plume Particle Size Measurements in Solid Propellant Micromotors

D. Laredo,* J. D. McCrorie II,† J. K. Vaughn,‡ and D. W. Netzer§
Naval Postgraduate School, Monterey, California 93943

Particle size distributions were measured in the chamber, nozzle, and plume of a subscale solid propellant rocket motor. A significant reduction in the mean size of the aluminum/aluminum oxide particles occurred within the motor chamber. The mass fraction of small particles (<2 μ) at the nozzle entrance was less than 10%. Also, most particles were smaller than 50 μ, although a few as large as 85 μ were present. In the converging and throat portions of the nozzle it appeared that particle breakup dominated over collision coalescence. Collision coalescence was observed to occur more dominantly in the supersonic nozzle flow. At the nozzle exit the particle mean size was usually less than 2.5 μ. The particle size distributions were bimodal or trimodal, with the larger particles concentrated near the plume centerline. Because of the short nozzle residence times it is not known whether or not these results are also applicable to full-scale motors. The mean size of the small Al_2O_3 particles in the plume edges was less than 0.5 μ in diam, with an index of refraction of 1.64 ± 0.04 (apparently γ-Al_2O_3), independent of propellant composition, motor operating conditions and nozzle geometry.

Introduction

ALUMINUM in solid rocket propellants is a highly desirable ingredient for many applications.[1] Although the condensed products of metal combustion are required for good combustion efficiency, they also create disadvantages such as slag accumulation, losses in performance, and an overradiating exhaust plume. The size distribution of these particles strongly affects all of the processes in the combustion chamber, exhaust nozzle, and in the near field and far field of the plume.

There is little reported data on the size distributions of the particles at the entrance and exit of the nozzle and within the plume, although knowledge of these distributions is essential for accurate prediction of plume signature and motor performance.[2]

Most particle size distribution data have been obtained from collected motor exhaust particles or from strands burned in combustion bombs in which the particles (quenched or unquenched) are captured and analyzed. The limitations of these methods lead several authors[3,4] to discuss the validity and the applicability of such results to the internal ballistics of real motors. In the combustion chamber, most reported results indicate that the particles are present in at least two modes. The first mode is thought to be a log-normal distribution with a mode peak below 2 μ in diam, and to contain about 65–85% of the oxide mass.[3,5] The second mode is also thought to be log-normal with particles between 5–150 μ, although particle diameters up to 500 μ have been reported. A recent investigation[6] using quenched and unquenched combustion products and exhaust plume light scattering measurements has indicated that the nozzle entrance size distribution is trimodal with modes at 1.7, 9, and 45 μ.

The nozzle/plume flowfield codes[7,8] predict that the particle size distribution within the plume is not uniformly distributed in the radial direction. Particles larger than approximately 5 μ are shown to be concentrated along the plume centerline, failing to follow the rapid gas flow turning that occurs in the nozzle throat region. Even particles as small as 1.0 μ are predicted not to follow the flow along the diverging nozzle wall. Thus, it is expected that particles in the outer regions of the plume will be less than 1.0 μ in diam. The smaller particles are generally predicted to be nearly in thermal equilibrium with the surrounding gas. In this case, if the equilibrium exhaust temperature from the nozzle is somewhat less than 2318 K (alumina melting point), it is reasonable to assume that the smaller particles are solids. If supercooling of the particles occurs before solidification, the particles could remain liquid for several exit diameters into the plume. The larger molten particles are thought to be limited to the central region of the plume. Solid Al_2O_3 is known to have considerably lower emittance than liquid Al_2O_3. Thus, if small solid particles are prevalent in the outer regions of the plume, they can have a dominant effect on the plume signature.

Most of the modeling for plume radiation has used an arbitrary particle size distribution with sizes in the very small range, 0.1–2 μ, and some up to 5 μ. Strand et al.[9] did report a bimodal distribution in the plume, but from speculative argumentation only. Traineau et al.[6] have reported a bimodal distribution with modes at 3 and 20 μ. Laredo and Netzer[10] have reported quadramodal distributions with modes at <2, 5, 10, and 20 μ. The code qualified as the state-of-the-art for the calculation of the infrared radiation emitted by exhaust plumes has been validated only for a factor-of-two accuracy over the 2–25-μm spectral range.[11] This inaccuracy is in part due to the lack of data on the particle size distribution and on the optical properties of the particulate matter in the exhaust environment, both of which can vary in the radial and axial directions. For engineering purposes, a semi-empirical formula[2] is often used to specify the mean size of the Al_2O_3 exiting the exhaust nozzle. Phenomena such as collision coalescence, breakup, lag between the particle and gas velocities, and temperatures and stratification of the particle sizes all can occur in the exhaust nozzle. The spatial distribution of the two-phase flow in the plume is also of primary importance for the prediction of the plume signature due to the phenomena associated with the plume optical depth.[12] With increasing optical depth plumes undergo a transition from emitting in proportion to their volume to effectively emitting from a cylindrical surface. The particle size distribution can

Received Dec. 11, 1991; revision received June 1, 1993; accepted for publication Nov. 22, 1993.

*Research Associate, National Research Council.
†Graduate Student, Lt. U.S. Navy.
‡Graduate Student, Capt. U.S. Army.
§Professor. Member AIAA.

also affect the radiation through the effects of the scattering cross section. These effects make the use of mean size data probably not appropriate and/or adequate for many plume signature and motor performance calculations.

Several researchers have reported experimental data on the optical and infrared properties of alumina at elevated temperatures, and yet there is considerable confusion due to the discrepancies (the imaginary part of the index of refraction reported in the literature varies from 3×10^{-2} to 10^{-7}). In motor and nozzle flows gaseous species can easily mix into the molten alumina, making the absorption coefficient of the particles depend on the propellant composition. Rieger[13] and Pluchino and Masturso[14] calculated the emissivity of contaminated Al_2O_3 (with unburnt Al, C). They showed that very small amounts of carbon or aluminum on/in an alumina particle can greatly increase the particle emissivity.

Another aspect that can affect the optical properties of the alumina in plumes is the crystal phase. The general indication is that the smaller particles tend to be gamma phase and the larger ones alpha phase. Dill et al.[15] suggest that the alpha-to-gamma ratio may depend upon the temperature-time history of the particle. The optical properties may also be size dependent since the real part of the index of refraction has been found to decrease with particle size. In the plume, most of the particles are small with an expected lower index of refraction.

This article is a summary of several individual investigations which have been conducted to obtain particle size distributions and some optical properties from the propellant surface to the plume near field.

Experimental Methods

Overview

Several diagnostic techniques have been used for measurements of the particle size distributions and optical properties produced by small axisymmetric motors. In situ diagnostic techniques included ensemble and single particle sizing instruments and multiple-wavelength extinction measurements. Special techniques have been developed to provide clean optical paths for forward scattering measurements inside the rocket motor chamber and through the plume; the latter with a combined optical/collection probe.[16] Particles collected using plume probes, as well as those collected from the walls of the combustor and exhaust nozzle, have been examined using a scanning electron microscope. The diagnostics currently in use with the axisymmetric motor are shown in Fig. 1.

Propellant Configuration and Motor Conditions

A small axisymmetric motor was used for most of the investigations with an end-burning or radial burning grain configuration. It had an internal diameter of 5.1 cm. Motor length could be varied, but for most tests it was 25.4 cm, providing a residence time of 30–50 ms. The motor incorporated nitrogen purged viewing windows located either 2 cm from the propellant surface or at the nozzle entrance. To keep the windows clean required a nitrogen flow rate of approximately 10% of the propellant mass flow rate. Thus, when measurements were taken through one set of windows, no further particle size measurements were made downstream. The exhaust nozzles were constructed either of copper or graphite with a 45-deg converging half-angle and a 15-deg diverging half-angle. Throat diameter was varied (nominally 0.5 cm) to control the chamber pressure. Following the work of Traineau et al.,[6] another motor was constructed with the addition of a helium quench manifold 10 cm from the motor head-end. The idea in this case was to quench the particulates within the motor (hopefully without shattering the particles) so that they would not change in size distribution into the plume. In this way nozzle exhaust measurements (which are easier to make than through-motor measurements) could be used to measure the in-motor particle size distribution. A helium flow equal to 30% of the propellant gas mass flow was required to reduce the temperature of the propellant gases to approximately 2000 K. The helium injection Mach number was 0.87, and the throat had to be enlarged to maintain the same desired operating pressure.

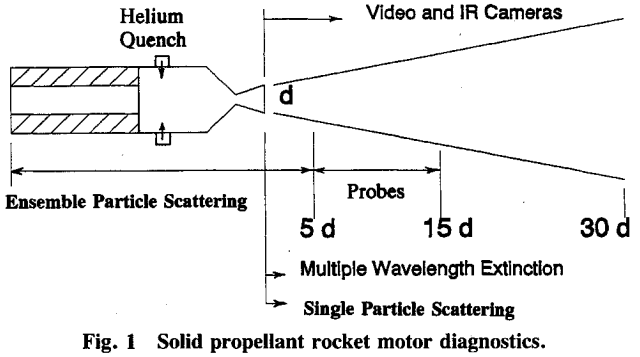

Fig. 1 Solid propellant rocket motor diagnostics.

Three propellants have been used (two provided by the Air Force Phillips Laboratory and one by the Thiokol Corp.), with either 2, 4.69, or 16% aluminum by weight (Table 1). The first two propellants utilized a glycidyl azide polymer (GAP) binder, whereas the 16% aluminum propellant used a polybutadiene-acrylonitrile-acrylic acid (PBAN) binder. The 16% propellant had a significantly lower burning rate and the gases produced contained much more hydrogen and carbon monoxide because more oxygen was tied up by the Al_2O_3 product. The end-burning grain was most often 2.54 cm in length and the radial burning grain most often utilized a 0.95-cm web.

Impact Probe

A stainless steel wedge covered with a copper sheet was exposed to the rocket plume for 0.5 s. It employed a flat front surface and tapered sides to provide different particle impact situations. The copper could be removed after the test and placed directly under the scanning electron microscope (SEM). The SEM pictures were generally used only to provide qualitative data, e.g., the maximum and minimum observable sizes and the most prevalent size.

Multiple Wavelength Extinction Apparatus

Multiple wavelength extinction measurements can be used to determine particle optical properties and the Sauter mean diameter D_{32}, if something is known about the shape of the size distribution, and (for visible and uv light) if most of the particles are smaller than about 1 μ. The current system used a collimated mercury-xenon white light source (with 10 strong peaks between 253–579 μ) with a Oriel Model 77400 Multispec Spectrograph. A 1024 element diode array was used to record the transmitted intensities at each wavelength. The response characteristics of the diode permitted six lines between 334–577 μ to be utilized. Thirty-two scans were made at 500 KHz for each test.

A Mie code[17] was used to generate mean extinction coefficients for a specified distribution, particle relative refractive index, and absorption coefficient $m = a - ib$, and wavelength λ. The transmission law for a polydispersion[18] is given by

$$T = \exp[-(3\bar{Q}C_m L)/(2\rho D_{32})]$$

T is the transmittance at a specified wavelength, $\bar{Q}$ is the mean extinction coefficient, C_m is the mass concentration of particles, L is the path length containing particles, ρ is the particle density, and D_{32} is the Sauter mean diameter. Thus, assuming m independent of λ

$$\text{Experimental} \qquad \text{Theoretical}$$
$$\ln(T_{\lambda i})/\ln(T_{\lambda j}) = \bar{Q}(\lambda i, D_{32}, m)/\bar{Q}(\lambda j, D_{32}, m)$$

Table 1 Propellant compositions and properties

Ingredients, wt %	Propellant DD1	DD5	TP-H1148
Aluminum, size, μ	2.0 (5–20)	4.69 (5–20)	16.0 (7.5–84)
AP	47.45 @ 200 μ	45.7 @ 200 μ	48.8 @ 200 μ
	25.55 @ 25 μ	24.61 @ 25 μ	20.9 @ 30 μ
GAP (200-1)	14.67	14.67	—
PBAN	—	—	14.0
TEGDN	8.49	8.49	—
TEPANOL	0.15	0.15	—
N-100	0.845	0.845	—
HDI	0.845	0.845	—
Fe_2O_3	—	—	0.2
Burning rate exp.	0.362	0.442	0.35
Density, g/cc	1.744	1.756	1.778
Burning rate @ 5.18 MPa, mm/s	16.4	20.1	10.0

Assuming, e.g., a log-normal distribution, calculations for the mean extinction coefficients were made for various values of m, standard deviation of the distribution σ_g, and D_{32}. The unknowns were D_{32}, a, b, and σ_g. The measured λ-transmission ratios were plotted against the calculated mean extinction coefficient ratios (e.g., 6 lines provide 15 independent λ-transmission ratios), and a regression analysis was used to determine the values for the four unknowns that best fit the line with a 45-deg slope. The accuracy of this method for measuring small particles improves with shorter wavelengths and with wider spacings between the wavelengths.

Using the Mie code for extinction coefficients and the transmission law it can also be shown that if 5-μ particles are present with 0.1-μ particles, the measured transmittances and calculated D_{32} will not be significantly effected by the larger particles if the volume of the smaller particles is at least 2.5 times the volume of the larger particles. SEM analysis of collected particles indicated that this condition was satisfied in the edges of the plume.

Malvern Particle Sizing Instruments

Two Malvern systems were used, the 2600 HSD[19] and the Mastersizer.[20] The 2600 HSD uses forward scattered light with a maximum angle of approximately 14 deg. It is based entirely on Fraunhofer diffraction, which limited the accurate determination of particle size to those with diameters greater than 1.2 μ (with an estimate of the volume % to as small as 0.5 μ). The Mastersizer measures forward scattered light to approximately 50 deg. It employs Mie corrections to the diffraction theory (requiring inputs of relative index of refraction and the absorption coefficient), and permits particles as small as 0.5 μ to be measured in gases.

The required proximity of the range (Fourier transform) lens to the particles severely restricts the use of the instrument for the rocket motor environment. It cannot be used remotely (with fiber optics) and the size of the motor or portion of the plume that can be sampled is quite small. The instrument must also be protected from the plume environment, and measurements require the maintenance of clean lenses and viewing windows.

Beam steering from density gradients in the flow causes some difficulties, as it will for any technique based upon forward scattering at small angles. It is evidenced by a Gaussian light intensity profile on the first few diodes of the array. The voltages from the affected diodes are discarded before attempting to find the best theoretical scattering intensity profile to fit the measured profile. This reduces the upper limit of particle size that can be accurately measured. However, the sizes effected are generally larger than observed to occur in motors and plumes.

The instruments are quite accurate for both locating the mode peaks and determining the distribution shape when obscurations are less than 50%. At higher obscurations, multiple

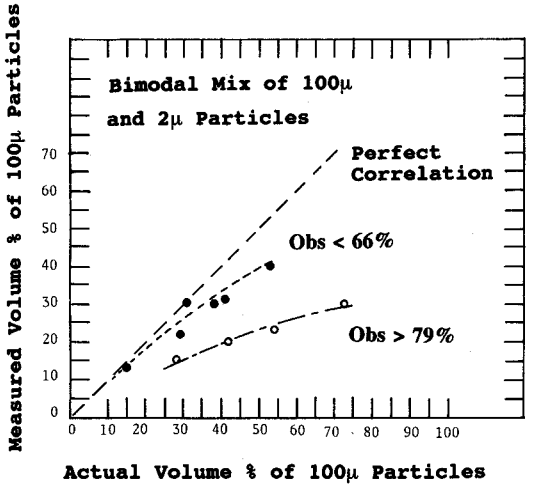

Fig. 2 Measured (Malvern) vs actual volume percentage of 100-μ particles in a bimodal mixture with 2-μ particles.

scattering effects result in the measured value of D_{32} being less than the actual D_{32}. However, we have found that the mode peaks continue to be accurately determined. Calibrations using suspended spheres with bimodal distributions (Fig. 2) showed that even when the large particles occupy only 15% of the particle mass in highly opaque environments they will be detected.

One other caution should be mentioned. When the Malvern is used to measure particles in a reacting environment, significant radiation from the combustion process can be at the laser wavelength. In many other applications this can be handled by chopping the input light and phase-locking it with the detected signal. When using the Malvern, a laser line filter must be employed in front of the range lens. Since these filters pass less light with increasing incidence angle, they can distort the scattered light intensity profile in favor of larger particles. Thus, laser line filters should be as wide-pass as possible and the effects introduced by them should be determined using calibration reticles and/or microspheres of known size distribution.

Thus, although the Malvern instruments have many shortcomings for use in the rocket motor environment, if properly used they can provide valuable and accurate data over a very large dynamic range and in very high velocity environments.

Single Particle Analyzer

The single particle analyzer used in the present effort was manufactured by Spectron Development Laboratories, Inc. in 1988.[21] It has the capability to measure the diameter and velocity of individual particles (passing through the measurement volume) from 0.5 to 5 μ and up to 2000 m/s, respectively.

The maximum permissible number density is $10^6/cm^3$. A 4-W argon laser (514.5 nm) was used to produce a laser sheet which passed through the exhaust plume. The approximately cylindrical probe volume was 50 μ in diam × 380 μ in length. Because of the 2000 m/s limit, the test series conducted using this instrument utilized a highly underexpanded nozzle flow.

Results and Discussion

Particle Size Distributions, Propellant to Plume

Earlier experiments[16,22-26] used both two- and three-dimensional motor geometries and additional additives to aluminum. The nozzle expansion ratio in this series of tests provided slightly underexpanded to ideal expansion conditions. A summary of the results is presented in Table 2. The results show a significant change in the particle *mean size* within the motor chamber, from about 130 μ, on or near the propellant surface, to 4–17 μ at the entrance of the nozzle. The measured D_{32} of 132 μ was in good agreement with the quench bomb data reported in Refs. 3 and 27. At the nozzle exit the particle mean size remained in the lower limit size range (submicron to micron) of the diagnostic device (Malvern 2600 HSD with a 100-mm range lens). The mass fraction of particles smaller than 2 μ at the nozzle exit was found to be 8–35% for pressures greater than 3.2 MPa, in some contrast to other reported results[6] where the mass fractions were less than 10%. It should be noted that the particle breakup requires not only the attainment of a critical Weber number but also time at this condition. In this regard, the subscale motor with similar geometry to a full-scale motor results in significantly less nozzle residence time. This may result in different nozzle exit particle diameters for the subscale and fullscale motors.

The overall trend in mean size does not imply that larger particles were not present (see modes in Table 2). Larger particles were always present in the motor chamber (up to 200 μ near the propellant surface and 84 μ at the nozzle entrance), and within the plume (up to 32 μ across the centerline and up to 5 μ at the edges) when measured optically.

Table 2 Summary of particle size data

	D_{32}^{D43}		
	Vol. % < 2 μ Peaks of Volume Distribution		
P_c, MPa	Propellant surface	Nozzle entrance	$5d_e$
		16% Aluminum	
1.38			$1.6^{4.6}$ $_{53\%}$2, 12
1.80		$3.9^{5.3}$ $_{7\%}$3, 7	
3.60	132		
		5% Aluminum	
1.80			$1.3^{2.3}$ $_{5\%}$2, 8, 15$_{weak}$
2.90		$4.8^{6.0}$ $_{1\%}$2, 3, 8	
4.3			$2.0^{4.3}$ $_{35\%}$2, 4, 13
5.0		$4.3^{5.7}$ $_{5\%}$2, 3, 7	
		2% Aluminum	
1.80			$1.7^{8.0}$ $_{50\%}$2, 7, 27
2.20		17.3^{29} $_{0.2\%}$2, 3.5, 7, 18, 43	
2.90		$3.7^{5.3}$ $_{9\%}$2, 6, 11$_{weak}$	
3.2			$5.2^{12.3}$ $_{8\%}$2, 8$_{weak}$, 18
5.7		$4.9^{5.8}$ $_{0.5\%}$3, 7	

However, SEM pictures of particles collected from the converging walls of the exhaust nozzle revealed no particles larger than 40 μ.

More detailed presentations of the Malvern data obtained at low pressures are shown in Figs. 3–6. These figures present the volume (or mass) of the particles in each size range relative to the total volume of all the particles present in the measurement volume divided by the width of each size range vs the geometrical mean diameter of each size range. At the

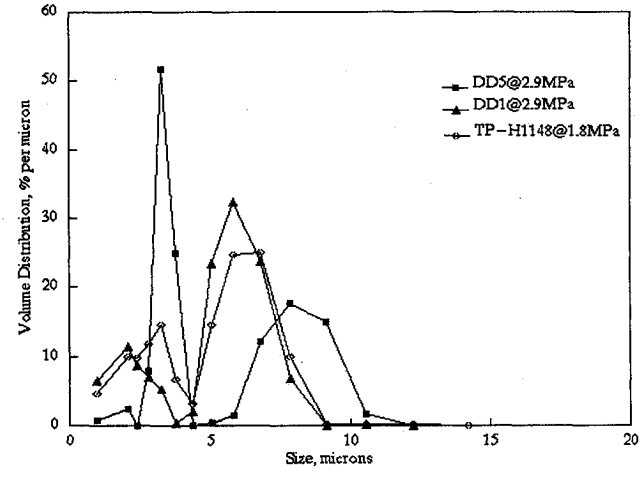

Fig. 3 Particle size distributions at the nozzle entrance at low pressure for the 2, 5, and 16% aluminum propellants.

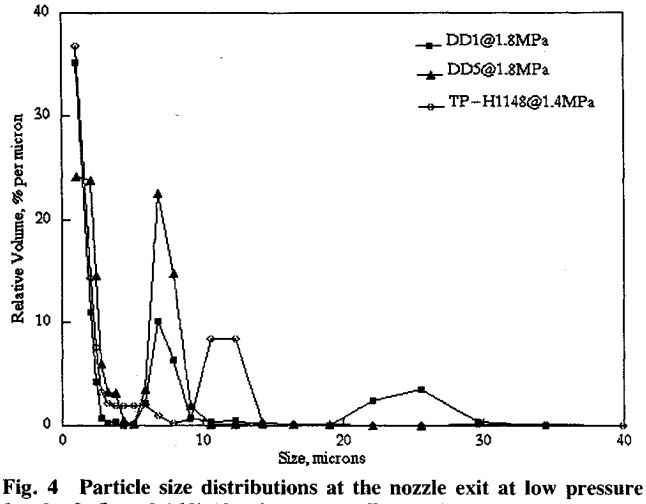

Fig. 4 Particle size distributions at the nozzle exit at low pressure for the 2, 5, and 16% aluminum propellants.

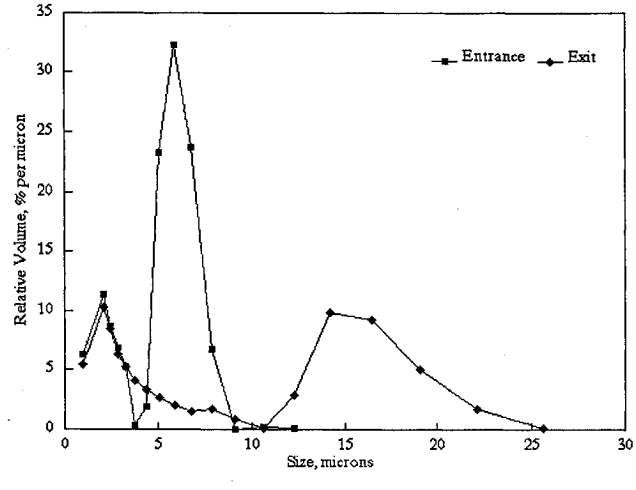

Fig. 5 Particle size distributions at the entrance and exit of the nozzle at low pressure for the 2% aluminum propellant.

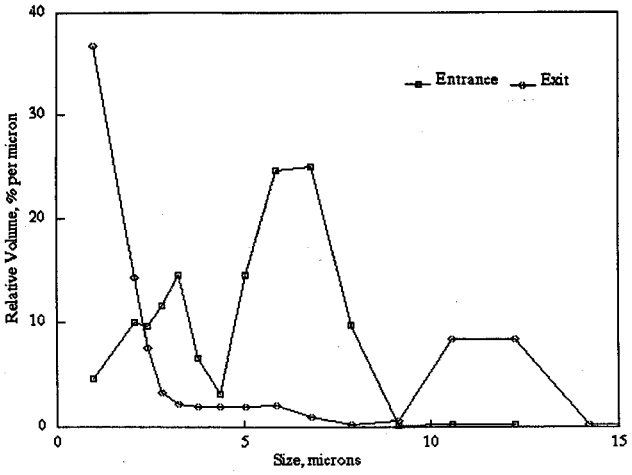

Fig. 6 Particle size distributions at the entrance and exit of the nozzle at low pressure for the 16% aluminum propellant.

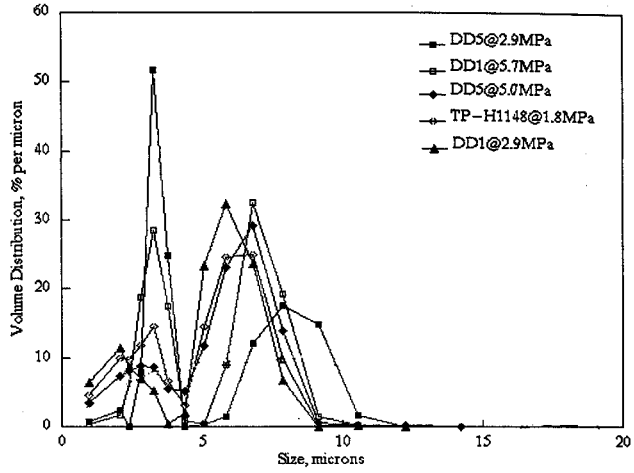

Fig. 7 Particle size distributions at the nozzle entrance at various chamber pressures for the 2, 5, and 16% aluminum propellants.

nozzle entrance (Fig. 3) the particle size distribution was usually bimodal (with mode peaks between 2–3 μ and between 6–8 μ), with about the same volume concentration in each mode. There may also have been an additional mode below 0.5 μ (outside the Malvern measurement range). In the plume the distribution was bimodal or trimodal (Fig. 4), often with significant volume concentrated in the smallest mode. The volume in this mode appeared to vary both with chamber pressure and aluminum loading. Even if only a small part of the volume of the particles in the plume were concentrated in larger particles (20–30 μ), their appearance should be the result of a "growing" process in the nozzle. However, another possibility existed; the slag formed on the convergent part of the nozzle flowed toward the throat and was expelled from it at low frequencies (as observed on a video camera).

The SEM pictures of the collected particles from the convergent part of the nozzle showed two different surface appearances of the large particles (from 10 to 15 μ). Some were spherical particles with numerous small particles (size ratio of 1–10) well aligned, in concentric circles, on the surface. This arrangement could be explained in two possible ways. First, if the particles are very small (about 0.1 μ) they may be the result of the condensed products that occur on the surface during the burning of the agglomerate. However, if they are larger (about 1.0 μ) they should be the result of a collision process. The other particles were almost spherical (15–20 μ in diam) with striations on their surface. This could be the result of the progressive accumulation of the aluminum oxide on the burning particle surface which was pushed to the lobe right after it was formed. The progressive solidification of these layers could show this striate appearance.

Figure 5 shows a comparison of the particle size distributions for the 2% Al propellant (with 3 MPa chamber pressure) at the entrance and the exit of the nozzle. At the entrance of the nozzle the first mode was between 1–4 μ, and the second mode was between 5–8 μ, with a relative volume concentration 3.3 times that of the first mode. In the plume the first, second, and third modes were between 1–4 μ, 5–8 μ (weak), and 12–25 μ, respectively, with relative (to the volume of the small range) concentrations of 0.15 and 1.0. It appears that across the nozzle more smoke is generated together with the formation of large particles. The same phenomena is presented in Fig. 6 for the 16% Al propellant.

Figure 7 shows that the particle size distribution at the nozzle entrance was about the same for all the end burning propellants and for all the tested pressures. In these small rocket motors with end burning grains and long residence times the particle size distribution at the entrance of the nozzle was practically invariant with the conditions in the chamber (pressure and propellant formulation).

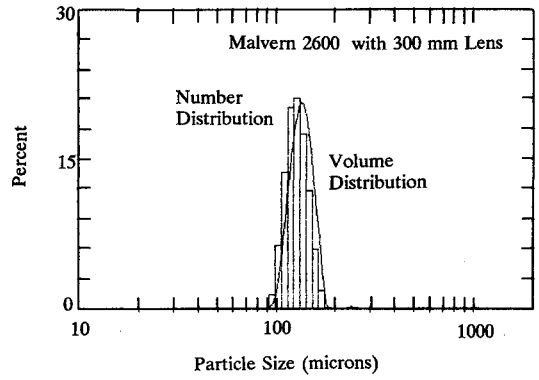

Fig. 8 Particle size distribution near the propellant surface at a pressure of 3.6 MPa for the 16% aluminum propellant.

The invariance of the particle size distribution and the absence of very large particles (>85 μ) at the entrance of the nozzle of the small motor used in this investigation could result either if no agglomeration process occurred on the propellant surface, or if the size of the agglomerates had been reduced considerably due to the long residence time (about 40 ms) of this particular motor chamber. In order to verify the occurrence of agglomeration on the propellant surface, the particle size distribution was measured 2.0 cm above the regressing surface of TP-H1148 by shortening the length of the combustion chamber. As shown in Fig. 8, the particles leaving the propellant surface at 3.6 MPa were normally distributed with a mean diameter D_{32} of 132 μ and a standard deviation of 18 μ. These agglomerates were significantly larger than the original ingredient Al powder. This result was clear evidence of the agglomeration process. These results together with those presented in Fig. 6 indicate that almost all the agglomerates were converted to much smaller particles during their trajectories along the length of the combustion chamber.

The residence time in the combustion chamber, in most of the experiments, was about 40 ms. This indicates that the consumption/burning of the agglomerates initially formed on the propellant surface cannot explain the reduction in D_{32} from 132 μ to 4–17 μ. Two possible explanations could be considered: 1) the diffusion limited droplet burning model is not applicable to the agglomerates in the propellant gas environment, 2) or a breakup mechanism (multiple shedding of lobes, etc.) occurred even at the low Mach numbers and low accelerations present in the motor. It should be reemphasized that the above variations in mean particle size only show the trends in particle size with position.

Comparison of Results from Different Diagnostic Techniques

In the data presented above there was some concern that the high obscurations observed through the motor were resulting from the presence of soot (from inhibitor charring) and/or smoke particles entering the window purge cavities. These conditions can obscure the presence of a small number of larger particles, which may represent a significant volume (mass) of condensed material. In the tests conducted for the following set of data the window purge rate was increased and attempts were made to minimize the quantity of inhibitor/bonding compound that was used.

In this portion of the investigation the 2% aluminized propellant was used in an end-burning grain operated at a nominal pressure of 2.2 MPa with a highly underexpanded nozzle (p_e = 0.7 MPa). Size distributions in the exhaust plume (at 8.9 exit diameters) were measured using the Spectron Single Particle Analyzer, the Malvern 2600 HSD ensemble particle sizer, and by SEM examinations of particles collected on the impact probe. Size distributions inside the motor were measured using the Malvern 2600 HSD through windows at the nozzle entrance (with increased window purge rate), SEM examination of particles collected from the walls at the nozzle entrance, and exhaust plume measurements when the motor combustion products were quenched with helium gas. The underexpanded nozzles were used to limit the exhaust velocity to below the upper limit of 2000 m/s of the single particle analyzer.

Nonquenched Motor Particle Experiments

A summary of the results obtained without helium quench in the motor (repeated tests) are presented in Fig. 9.

Beam steering of the Malvern laser beam in the plume resulted in a maximum detectable particle size of approximately 82 μ (capturing all of the first Airy diffraction ring). There was a bimodal distribution of particle sizes with modes at less than 2 μ and approximately 3.5 μ. The maximum size observed was 4.3 μ. The Sauter mean diameter D_{32} was 2.5 μ, and the mass-weighted average diameter D_{43} was 3.1 μ. With 87% of the particles (number) less than 2 μ and none larger than 4.3 μ, the Malvern results were in good agreement with the single particle counter measurements in the plume. Particles collected on the impact probe had sizes between 0.2–2.3 μ, with the majority of particles being smaller than 0.5 μ. Considering that the Malvern estimates particles only to a minimum of 0.5 μ and that this was also the lower limit of the single particle counter (SPC), the sizes were in good agreement. In the plume of the highly underexpanded nozzle flow the mode at >15 μ observed above with underexpanded or ideally expanded flows was not observed.

Through-motor data obtained with the Malvern resulted in an apparent obscuration of 95%. The approximate volume concentration of particles in the motor was 3×10^{-5}, based on the propellant burning rate and chamber pressure. With D_{32} = 17 μ, as measured by the Malvern, the obscuration should have been only approximately 22%. Thus, it was apparent that either some beam steering was present (giving a false transmittance) or a large amount of small particles (soot, etc.) was present. Soot deposits were not observed on the motor walls or in the collected plume particulate. Beam steering apparently occurred, but it was overpowered by the intensity of the scattered light reaching the inner diode rings. It was concluded that the beam steering did not significantly affect the measured intensity profile, but that the actual obscuration was much less than the indicated 95%. The maximum detected size was 84 μ, D_{32} was 17 μ and D_{43} was 29 μ. The modifications in test procedures discussed above did apparently permit the small number of particles larger than 11 μ to be detected.

Particles were scraped from the converging wall of the nozzle and examined using the SEM. The maximum particle size observed was 40 μ and the smallest was 0.5 μ. The particles were primarily distributed in four sizes; 0.7, 2, 6, and 25 μ. Most particles were 0.7 and 2 μ. The Malvern indicated that most of the particles (number) were smaller than 2 μ, in agreement with the collected particles. The Malvern also indicated a mode peak at 43 μ (e.g., a significant number of particles), in agreement with the maximum size from the SEM of 40 μ.

Each of the diagnostic techniques employed had different dynamic ranges. With this in mind, all of the results were in quite good agreement.

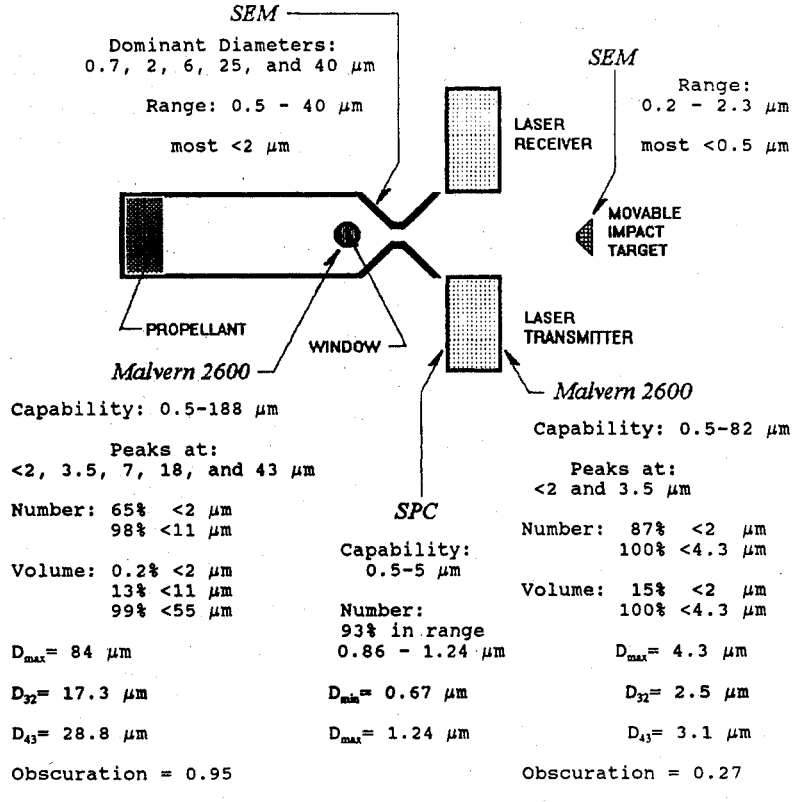

Fig. 9 Particle sizes for the 2% aluminum propellant from multiple diagnostic methods, nonquenched.

Quenched Motor Particle Experiments

A summary of the results obtained with a helium quench in the motor is presented in Fig. 10. The single particle analyzer detected particles ranging in size from 0.48 to 1.43 μ. Of these, approximately 86% were 0.67–1.05 μ. The maximum size detected by the Malvern in the plume was 30 μ, D_{32} was 3.2 μ, and D_{43} was 13.8 μ. The mode peaks were at <2, 2, 4.5, 12, and 26 μ. With 95% of the number of particles less than 2 μ, the Malvern and SPA results were in reasonably good agreement. The SPA could not detect the very few number of large particles due to both the dynamic range limitations and to the highly improbable event of a single large particle passing through the relatively small measurement volume.

The impact probe SEM pictures showed particles ranging in size from 0.3 to 2 μ, with the majority being smaller than 0.5 μ. This result was in good agreement with the Malvern and SPA measurements, although none of the few number of larger particles seen by the Malvern were observed.

For particles collected from the converging nozzle wall the maximum size observed was 59 μ and the minimum was 0.6 μ. The particles were primarily of five sizes; 0.7, 2, 7, 25, and 50 μ. Most of the particles were smaller than 2 μ. Since the Malvern did not detect particles larger than 31 μ in the plume, and the impact probe also saw only small particles, the implication was that the larger particles may not have been quenched to solid form before passing through the nozzle.

Comparison with Other Data

In this investigation, only a small amount of aluminum oxide was present (maximum of 3.8% by mass), the pressure averaged 2.2 MPa, there was significant residence time between the end-burning propellant grain surface and the nozzle entrance, and the plume measurements were made near the exit of a highly underexpanded (p_e = 0.7 MPa) nozzle.

The results obtained at the nozzle entrance were similar, and yet somewhat different (as discussed above) from the results reported above with the same propellant and approximately the same pressure. Those results (Table 2) had a higher mass percentage of <2-μ particles (approximately 9 vs 0.2%) and a smaller maximum particle size (12 vs 84 μ). Traineau et al.[6] reported (for a different propellant and operating conditions) approximately 10% of the mass in particle with diameters <2 μ, most particles smaller than 75 μ, and a maximum diameter of 120 μ. Although these results for the nozzle entrance vary somewhat for the different propellants and test conditions, they give a consistent picture. Most of the number of particles are smaller than 2 μ, but most of the mass (>90%) is contained in particles larger than 2 μ. Also, most particles are smaller than 50 μ, although a few as large as 80–100 μ are present.

At the nozzle exit with a highly underexpanded flow, the indication was that particle breakup dominated over agglomeration in the converging portion of the nozzle. The data in Table 2 (modes at larger diameters) indicate that significant agglomeration apparently occurs in the diverging section of the nozzle.

Plume Edge Particle Measurements

The objective of this portion of the investigation was to measure the particle mean size and index of refraction in the outer region of the plume where particles smaller than 1 μ are predicted to dominate the flow. Calculations with the Mie code showed that the mean extinction coefficient was insensitive to the absorption index for the expected values between 10^{-2} to zero. Thus, for calculation of the extinction coefficient, the aluminum oxide particles were considered to exhibit no absorption.

The exhaust plume was initially video recorded from above with a scaled plate beneath the plume to determine the ideal positioning for the measurements. An IR camera was also used to locate the afterburning region and the Mach disc locations within the plume. It was desired to make the transmission measurements in the outer regions of the plume to reduce the possibility of having large particles present, and to be out of the afterburning and Mach disc locations where high radiation intensity is present. However, it was necessary to be close enough to the exhaust nozzle to provide a steady

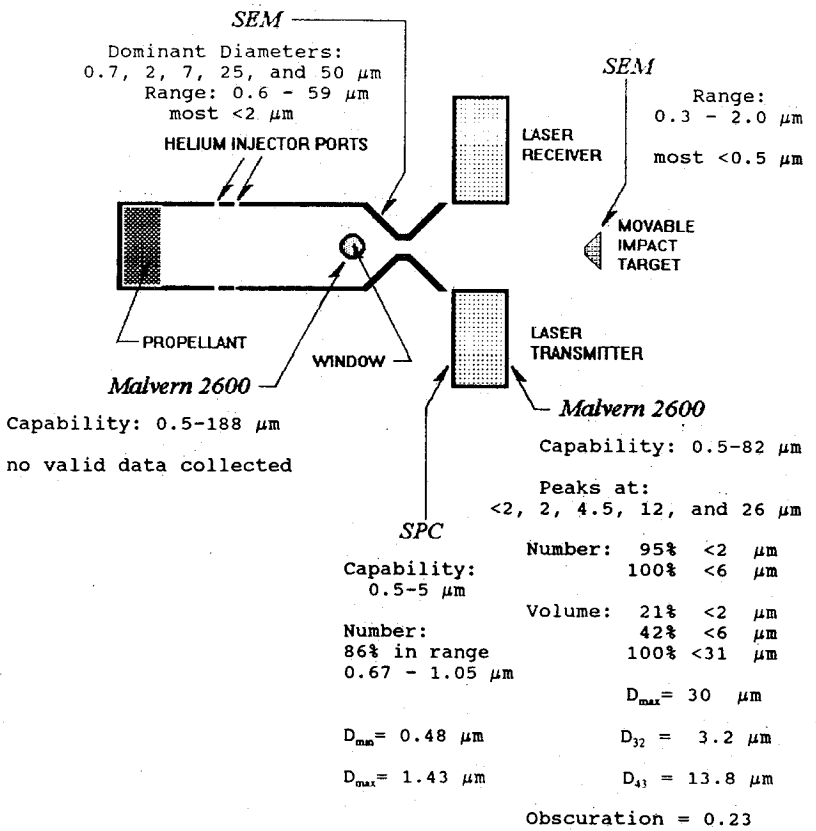

Fig. 10 Particle sizes for the 2% aluminum propellant from multiple diagnostic methods, quenched.

flow (relative to the sampling time). No significant radiation was detected at the wavelengths of the illumination source.

In an initial investigation[26] it was found for the 5% aluminum propellant very near the plume edge that

$$D_{32} = 0.150 \pm 0.006\ \mu$$

$$\sigma_g = 1.50 \pm 0.04$$

$$m = 1.63 \pm 0.13$$

The accuracy of the measured transmittance was approximately 0.5%. The uncertainty in D_{32} and σ_g were acceptable, but the uncertainty in m was higher than desired. The major reason suspected for this uncertainty (in addition to the data scatter expected from multiple firings) was the change in the motor operating conditions over the 240-ms recording time for eight sweeps of the photodiode array. Thus, the 33-KHz A/D was replaced with a 500-KHz A/D. This permitted 32 sweeps (for averaging) to be obtained in 70 ms.

In the present investigation (four tests) both the 5 and 16% aluminized propellants were used. To obtain higher pressures, radial burning grains were used in addition to end-burning grains. In addition, the diode array was modified to permit an additional line (334 nm) to be recorded. Various positions within the plume edge were also used in order to determine if the index of refraction varied significantly with pressure, propellant composition, or plume position. The 16% aluminized propellant also contained 0.2% Fe_2O_3 which could possibly affect the index of refraction of the particles.

It was found that none of the variables (P_c, nozzle area ratio, propellant composition, plume position) had a significant effect on the index of refraction. Only D_{32} changed as a result of changes in the plume position. Using the improved data acquisition with a broader range of test conditions resulted in

$$D_{32} = 0.30 \pm 0.02\ \mu$$

$$\sigma_g = 1.52 \pm 0.12$$

$$m = 1.64 \pm 0.04$$

The results of this investigation indicated that the small aluminum oxide particles that dominate the outer plume regions are probably γ-Al_2O_3, independent of propellant composition, motor operating conditions, and nozzle geometry. In addition, the good correlation of the data indicated that the small particles can be adequately represented by a monomodal, log-normal distribution.

Conclusions

1) To measure the particle size distributions and particle optical properties in solid propellant rocket motor chambers, nozzles and plumes require a variety of diagnostic instruments/techniques due to the very large range of particle sizes and concentrations present. Each instrument/technique has unique advantages and disadvantages, and specific size ranges which can be accurately measured. Agreements were good when the restrictions/operating limits of each method were taken into account.

2) The particle size distributions in the motor and within the plume are almost always multimodal, with a wide dynamic range. Subscale motor measurements indicate that, with long residence times aft of the propellant grain, the mass fraction of small particles ($<2\ \mu$) at the nozzle entrance is less than 10%. Most of the number of particles are smaller than 2 μ, but most of the mass (>90%) is contained in particles larger than 2 μ. Also, most particles are smaller than 50 μ although a few as large as 85 μ are present. Collisional processes within the chamber appear to remove many of the smaller particles.

3) A significant reduction in the particle D_{32} occurs within the motor chamber, from about 130 μ on or near the propellant surface to 4–17 μ at the entrance of the nozzle; indicating a breakup mode in the low Mach number chamber environment. It is not known whether or not this behavior also occurs in full-scale motors.

4) At the nozzle exit the mass fraction of the small particles varies with pressure and aluminum loading, but the particle D_{32} is usually $<2.5\ \mu$. The nozzle exit particle size distribution is bimodal or trimodal, with the larger particles concentrated near the plume centerline.

5) In the converging and throat portions of the nozzle it appears that particle breakup dominates over collision coalescence. Collision coalescence was observed to occur more dominantly in the supersonic nozzle flow. The short nozzle residence times for the subscale motors may result in different particle breakup behavior than present in full-scale motors.

6) The mean size of the small Al_2O_3 particles in the plume edges is $<0.5\ \mu$ in diameter with an index of refraction of 1.64 ± 0.04 (apparently γ-Al_2O_3), independent of propellant composition, motor operating conditions and nozzle geometry. The sizes can be adequately represented by a monomodal, log-normal distribution.

Acknowledgments

This work was supported by the Air Force Phillips Laboratory, Edwards AFB, California under MIPRs F04611-92-X-0327, F04611-93-X-000505, and F04611-93-X-000509, and by the National Research Council.

References

[1]Price, E. W., "Combustion of Metalized Propellants," *Fundamentals of Solid-Propellant Combustion*, edited by M. Summerfield, and K. K. Kuo, Vol. 90, Progress in Astronautics and Aeronautics, AIAA, New York, 1984, pp. 479–513.

[2]Hermsen, R. W., "Aluminum Oxide Particle Size for Rocket Motor Performance Prediction," *Journal of Spacecraft*, Vol. 18, No. 6, 1981, pp. 483–490.

[3]Salita, M., "Characterization of Al_2O_3 Particulate Formed During Combustion of SRB Propellant (TP- H1148)," Morton Thiokol Inc., Space Div., TWR-18456, Brigham City, UT, Sept. 1988.

[4]Cheung, H., and Cohen, N. S., "Performance of Solid Propellants Containing Metal Additives," *AIAA Journal*, Vol. 3, No. 2, 1965, pp. 250–257.

[5]Price, E. W., "Combustion of Aluminum in Solid Propellant Flames," *53rd Meeting of AGARD Propulsion and Energetics Panel, Solid Rocket Motor Technology* (Oslo, Norway), 1979, pp. 14-1–14-15 (AGARD-259).

[6]Traineau, J. C., Kuentzmann, P., Prevost, M., Tarrin, P., and Delfour, A., "Particle Size Distribution Measurements in a Subscale Motor for the Ariane 5 Solid Rocket Booster," AIAA Paper 92-3049, July 1992.

[7]Dash, S. M., Pearce, B. E., Pergament, H. S., and Fishburne, E. S., "Prediction of Rocket Plume Flowfields for Infrared Signature Studies," *Journal of Spacecraft and Rockets*, Vol. 17, No. 3, 1980, pp. 190–199.

[8]Hwang, C. J., and Chang, G. C., "Numerical Study of Gas-Particle Flow in a Solid Rocket Nozzle," *AIAA Journal*, Vol. 26, No. 6, 1988, pp. 682–689.

[9]Strand, L. D., Bowyer, J. M., Varsi, G., Laue, E. G., and Gauldin, R., "Characterization of Particulates in the Exhaust Plume of Large Solid-Propellant Rockets," *Journal of Spacecraft and Rockets*, Vol. 18, No. 4, 1981, pp. 297–305.

[10]Laredo, D., and Netzer, D. W., "The Dominant Effect of Alumina on Nearfield Plume Radiation," *Journal of Quantitative Spectroscopy & Radiative Transfer*, Vol. 50, No. 5, 1993, pp. 511–530.

[11]Nelson, H. F., "Influence of Particulates on Infrared Emission from Tactical Rocket Exhausts," *Journal of Spacecraft and Rockets*, Vol. 21, No. 5, 1984, pp. 425–432.

[12]Dash, S. M., Wolf, D. E., Beddini, R. A., and Pergament, H. S., "Analysis of Two-Phase Flow Processes in Rocket Exhaust Plumes," *Journal of Spacecraft and Rockets*, Vol. 22, No. 3, 1985, pp. 367–380.

[13]Rieger, T. J., "On the Emissivity of Alumina/Aluminum Composite Particles," *Journal of Spacecraft and Rockets*, Vol. 16, No. 6,

1979, pp. 438, 439.

[14]Pluchino, A. B., and Masturzo, D. E., "Emissivity of Al_2O_3 Particles in a Rocket Plume," *AIAA Journal*, Vol. 19, No. 9, 1981, pp. 1234–1237.

[15]Dill, K. M., Reed, R. A., Calia, V. S., and Schulz, R. J., "Analysis of Crystalline Phase Aluminum Oxide Particles from Solid Propellant Exhausts," *Journal of Propulsion and Power*, Vol. 6, No. 5, 1990, pp. 668–671.

[16]Racine, J. A., "Subscale Solid Rocket Motor Infrared Signature and Particle Behavior," M.S.A.E. Thesis, Naval Postgraduate School, Monterey, CA, Dec. 1991.

[17]Cashdollar, K. L., Lee, C. K., and Singer, J. M., "Three-Wavelength Light Transmission Technique to Measure Smoke Particle Size and Concentration," *Applied Optics*, Vol. 18, No. 11, 1979, pp. 1763–1769.

[18]Dobbins, R. A., Crocco, L., and Glassman, I., "Measurement of Mean Particle Sizes of Sprays from Diffractively Scattered Light," *AIAA Journal*, Vol. 1, No. 8, 1963, pp. 1882–1886.

[19]*Malvern 2600HSD Instruction Manual*, Malvern Instruments, Worchester, England, UK.

[20]*Mastersizer Instruction Manual*, Malvern Instruments, Manual Version IM100, Issue 3, Worchester, England, UK, Oct. 1989.

[21]"Particle Sizing Technique for Rocket Plumes," Spectron Development Lab., Inc., Rept. BMO-TR-88-73, Costa Mesa, CA, July 1988.

[22]Arnold, K. J., "An Experimental Investigation of Strand Burning Metallized Solid Propellants," M.S.A.E. Thesis, Naval Postgraduate School, Monterey, CA, Dec. 1989.

[23]Youngborg, E. D., Pruitt, T. E., Smith, J. M., and Netzer, D. W., "Light Diffraction Particle Size Measurements in Small Solid Propellant Rockets," *Journal of Propulsion and Power*, Vol. 26, No. 3, 1990, pp. 243–249.

[24]Brennan, W. D., Hovland, D. L., and Netzer, D. W., "Measured Aluminum/Aluminum Oxide Particle Behavior in a Subscale Solid Propellant Rocket Motor," *Journal of Propulsion and Power*, Vol. 8, No. 5, 1992, pp. 954–960.

[25]Butler, A. G., "Holographic Investigation of Solid Propellant Combustion," M.S.A.E. Thesis, Naval Postgraduate School, Monterey, CA, Dec. 1988.

[26]Kim, H.-O., Laredo, D., and Netzer, D. W., "Measurement of Sub-Micron Al_2O_3 Particles in Plumes," *Applied Optics*, Vol. 32, No. 33, 1993, pp. 6834–6840.

[27]Salita, M., "Quench Bomb Investigation of Al_2O_3 Formation from Solid Rocket Propellants (Part II): Analysis of Data," 25th JANNAF Combustion Meeting, CPIA 498, Vol. I, Oct. 1988, pp. 185–197.